

Article

Experimental Study of the Dynamic Performance of Steel Catenary Riser within the Touchdown Zone

Yang Yu ^{1,2}, Shengbo Xu ^{1,2,*} , Jianxing Yu ^{1,2}, Lixin Xu ^{1,2}, Xin Liu ^{1,2} and Pengfei Liu ^{1,2}

¹ State Key Laboratory of Hydraulic Engineering Simulation and Safety, Tianjin University, Tianjin 300072, China

² Tianjin Key Laboratory of Port and Ocean Engineering, Tianjin University, Tianjin 300072, China

* Correspondence: edwinb@tju.edu.cn; Tel.: +86-135-0212-8143

Abstract: This study proposed a novel experimental platform to conduct dynamic loading tests of a truncated model steel catenary riser (SCR) within the touchdown zone (TDZ). The facilities of the platform, including a soil tank, a loading system, and a soil stirring system, were introduced in detail. The parameters of the test were determined through the simulation of an in situ riser. A steel pipe was adopted as the model riser, with its outer diameter equaling that of the prototype SCR. Before executing the dynamic loadings, the model riser developed its static configuration under the submerged weight and applied bending moment. Subsequently, cyclic vertical and lateral displacement loads were applied to the truncated point. The test results showed that when the vertical loading amplitude increased from 200 mm to 300 mm, the stress ranges at the front of the model riser increased by more than 100%, whereas the stress range only differed by less than 5% under different loading periods. Numerical models of the SCR were built based on the vector form intrinsic finite element (VFIFE) method. High similarities between the test and simulation results proved the reliability of the nonlinear soil model and the numerical model. During the test, a seabed trench was developed with a depth of 0.71 D and a width of 0.48 D, and its shape was similar to the in situ trench.

Keywords: steel catenary risers; touchdown zone; dynamic loading tests; vector form intrinsic finite element method; riser–seabed interaction



Citation: Yu, Y.; Xu, S.; Yu, J.; Xu, L.; Liu, X.; Liu, P. Experimental Study of the Dynamic Performance of Steel Catenary Riser within the Touchdown Zone. *J. Mar. Sci. Eng.* **2023**, *11*, 151. <https://doi.org/10.3390/jmse11010151>

Academic Editor: Cristiano Fragassa

Received: 5 December 2022

Revised: 28 December 2022

Accepted: 29 December 2022

Published: 8 January 2023



Copyright: © 2023 by the authors. Licensee MDPI, Basel, Switzerland. This article is an open access article distributed under the terms and conditions of the Creative Commons Attribution (CC BY) license (<https://creativecommons.org/licenses/by/4.0/>).

1. Introduction

With the depletion of onshore and shallow-water petroleum resources, the untapped hydrocarbon reserves in deep water are becoming more attractive. The risers are the conductor pipes that connect the flow lines and floating platforms, and their integrities are of vital importance. Among the various kinds of riser systems, steel catenary risers (SCR) exhibit the advantages of high bearing capacity, high cost effectiveness, and simplicity in structure, making them one of the optimum solutions used in deep water [1]. Under the cyclic movement of the floating platform and environmental loads, the SCR may suffer from fractures induced by fatigue damage, especially within the joint connected to the platform and touchdown zone (TDZ) [2]. However, accurate prediction of the fatigue life of the SCR within the TDZ is challenging, owing to the uncertainties of riser–seabed interaction and the variation of seabed profiles.

Some theoretical and numerical analyses of SCR adopt rigid or elastic seabed models, which produce unrealistic results of the fatigue performance of SCR [3,4]. Based on the pipe–soil interaction model tests, several advanced vertical riser–seabed interaction models have been proposed and integrated into the finite element models [5–8]. The degradation of soil caused by the disturbance of the riser segment can be recorded, and the suction force can be simulated. Based on the nonlinear riser–seabed interaction model proposed by Randolph and Quiggin [6], the effects of different seabed stiffness, suction ratio, and loading period

on the fatigue damage of SCR were analyzed [9]. A seabed trench was developed under the oscillation of the SCR within several months [10], which also affected the mechanical behavior of the riser. The trench could be artificially inserted into the numerical model using a mathematical formulation [11], and the fatigue damage of the SCR was reduced. Using the R-Q soil model, Shiri [12] proposed a method to develop the seabed trench automatically to ensure consistency between the trench and SCR. Simulation results proved that the developed trenches have detrimental effects on the fatigue behavior of the SCR. The trenches developed using an artificial formulation, step method, and automatic method were compared and inserted into the SCR model by Randolph et al. [13], and the dynamic simulations showed that the fatigue damage of the SCR was significantly affected by the trench shape. Since the static offsets and low-frequency motions of the floating platform also contribute to the trench formation, Yu et al. [14] compared the trench shapes developed under different vessel motions and studied the trench effects on the fatigue life of the SCR using the inserting method. Shoghi and Shiri [15] and Shoghi et al. [16] simplified the trench using sloped lines and figured out how the seabed trenches influenced the fatigue damage of the SCR. These nonlinear riser–soil interaction models and seabed trenches mainly focused on determining the vertical seabed resistances; however, sophisticated lateral soil models have not been proposed and applied. Therefore, experiments should be carried out to determine the effect of horizontal riser–soil interaction on the behavior of SCR. Furthermore, the reliability of the nonlinear vertical soil models in a global SCR model still needs to be verified through experimental analysis.

Although the full-scale model tests of SCR can provide convincing results [17], the cost of a single test is considerable, and the environmental loads cannot be controlled or recorded in detail. This hinders the comparison between the test and simulation results. By contrast, laboratory tests are reliable and cost-effective alternatives. The tests can be categorized into small-scale global tests, reduced-scale cut-off model tests, and centrifuge tests. For a small-scale global test, the whole SCR was modeled using a silicone tube, whereas the seabed was substituted by dry foam, wet foam, or glass [18]. Despite the global mechanical behavior of SCR being well represented, the interaction between riser and seabed clay or sand is oversimplified, and the stress variation within the TDZ cannot be obtained accurately.

Regarding the reduced-scale cut-off model tests, the riser is truncated above the seabed, and the lower part is treated as the object to study. The truncated point of the SCR is taken as the loading point where displacement loads are applied. PVC and PE pipes were selected as the optimum choices for the model riser owing to their low rigidity. The cylinder irons strung by steel wire ropes were input into the pipe to increase the submerged weight [19]. Both ends of the model SCR were modeled as hinged, allowing the riser to rotate freely. All these measures contributed to magnifying the deformation of SCR. The influences of heave motion-induced vibration were investigated by Wang et al. [19] and Hodder and Byrne [20], with clay and sand used as seabed soil, respectively. When cyclic sway motions were applied to the truncated point of model SCR, the seabed trench was widened and deepened [21]. After fixing the soil tank on the shaking table, the seismic loading condition can be simulated to study the dynamic stress variation of the SCR within the TDZ [22]. However, when the low-rigidity pipes were applied in the model tests, the stiffness ratio between the riser and soil was reduced. This would induce a larger stress range along the SCR and make it more difficult to determine the difference between the test result and the numerical simulation result. Once the small-diameter steel pipes were adopted in the model test, high-frequency vibrations would be significant [23].

Similar to the reduced-scale cut-off model tests, the centrifuge tests focus on part of the SCR within the TDZ. The feasibility of using a truncated model SCR in the test was verified by Bhattacharyya et al. through numerical analysis [24]. Possessing the advantages of increasing the gravity by a factor of more than 40, the experiment can simulate a full-scale riser using a small-diameter steel pipe without the need of choosing an alternative material to ensure the rule of similarity [25]. The combinations of surge and heave motions were

applied to the truncated point of the model SCR, and the time history of the bending moment [26] and the fatigue life [27] were presented and analyzed. Furthermore, the clayey soil can be prepared within a shorter period using a centrifuge [28]. The limitation of the centrifuge tests is that both the mechanical facilities and the data acquisition system require a higher level of precision and safety, which is hard to realize.

Although great efforts have been made to perform a more realistic model SCR test within the TDZ, the existing model tests still have some limitations. The first limitation is that the bending moment cannot be applied to the truncated point of the model SCR. For an in situ SCR, the bending moment increases significantly before reaching the touchdown point (TDP) and contributes to the deformation and stress variation of the SCR within the TDZ. The tests can be more accurate if the bending moment is included. The second limitation is that the model SCR may not well represent the mechanical behavior of the in situ SCR. Although the reduced-scale cut-off model tests are easier to realize compared with the centrifuge tests, plastic pipes or reduced-scale steel rods may not be the optimum options to simulate the deformation and stress variation of a full-scale SCR. Furthermore, the cyclic sway motions cannot be applied in the centrifuge tests. These limitations require a novel test system for the experiment of large-scale model steel risers. The bending moment and cyclic displacement should be applied simultaneously to the model SCR.

Combining the merits of the reduced-scale cut-off model tests and centrifuge tests, a novel experimental platform was proposed and constructed to perform dynamic model tests of the SCR within the touchdown zone. The layout of the platform was presented in this study, and the structure of each component was introduced in detail. Based on the equipment, a dynamic test of the model SCR was carried out under the combination of the bending moment and cyclic displacement loads. Different loading amplitudes and periods were adopted to determine their influences on the mechanical behavior of the riser. Numerical models were built based on the vector form intrinsic finite element (VFIFE) method, and the vertical nonlinear soil model was integrated into the model. High similarities between the experiment and simulation results proved the practicability of the test platform and the reliability of the nonlinear soil model.

2. Development of Test Platform and Experimental Equipment

2.1. Layout of the Test Platform

The layout of the test platform is shown in Figure 1. The platform consists of a soil tank, a loading system, and a stirring system for clayey soil preparation. A large-scale steel pipe with a diameter of 6 inches was adopted as the truncated model SCR. Each end of the pipe was welded with a flange to connect to the facilities. The axial position of the loading facility along the soil tank was adjusted to install the pipe and fixed before the experiment. The loading end of the SCR was fastened to the bending moment loading system, and the tail end was connected to the elastic support. The riser was free to rotate at the tail end, whereas the vertical and horizontal displacements were restricted. After applying the bending moment, the model SCR developed its static configuration. The rotational angle of the loading end of the SCR was restrained by a mechanical locking device and remained constant throughout the test, and cyclic displacement loads could be applied to investigate the dynamic behavior of SCR.

2.2. Soil Tank

The length, width, and depth of the reinforced concrete soil tank were 20.05 m, 3.6 m, and 2.05 m, respectively. Under the soil tank, 6 bored cast-in-place piles were constructed and connected using the foundation beams to improve their rigidity and prevent the decline or settlement of the tank. The side wall thickness of the soil tank was 300 mm to sustain the pressure of clay. The cross section of the tank and the arrangement of reinforcements are shown in Figure 2. The plan view of the soil tank is shown in Figure 3a. Within the moving range of the loading device, the angle steel with 50 mm thickness was fixed to the surface of each side wall using bolts and shear keys, as shown in Figure 3b. For the other part of

the tank, the track of the stirring system was arranged along the top of each side wall using the anchor plates. After construction, stainless-steel plates were installed on each surface of the tank for protection.



Figure 1. The layout of the test platform.

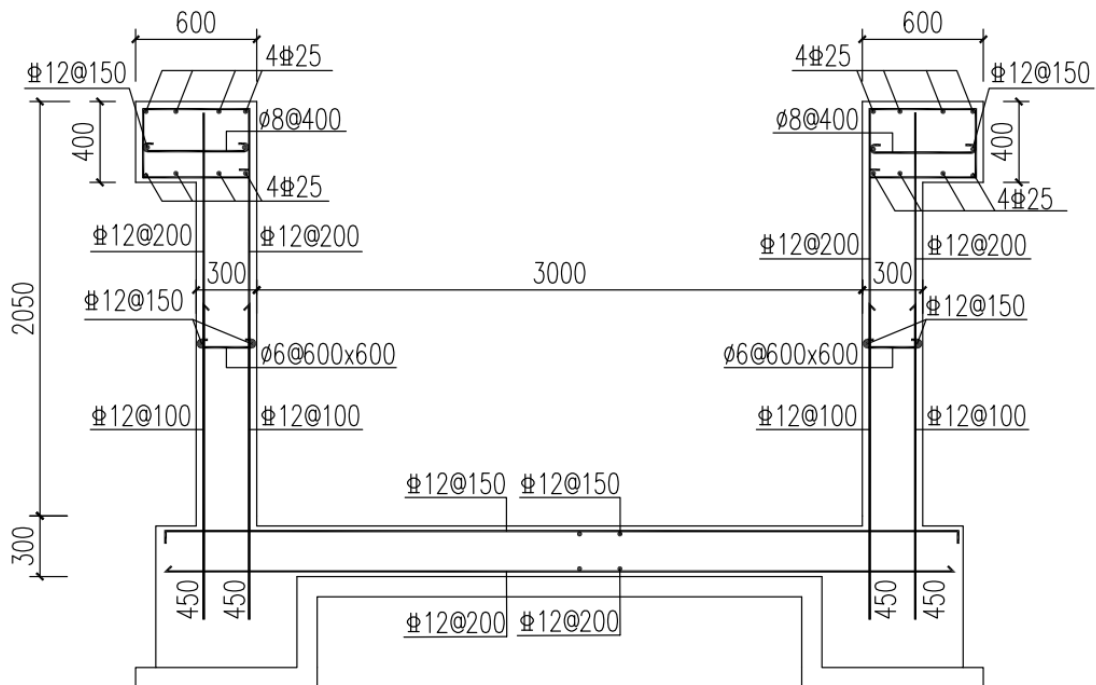


Figure 2. Reinforcement arrangement of the soil tank.

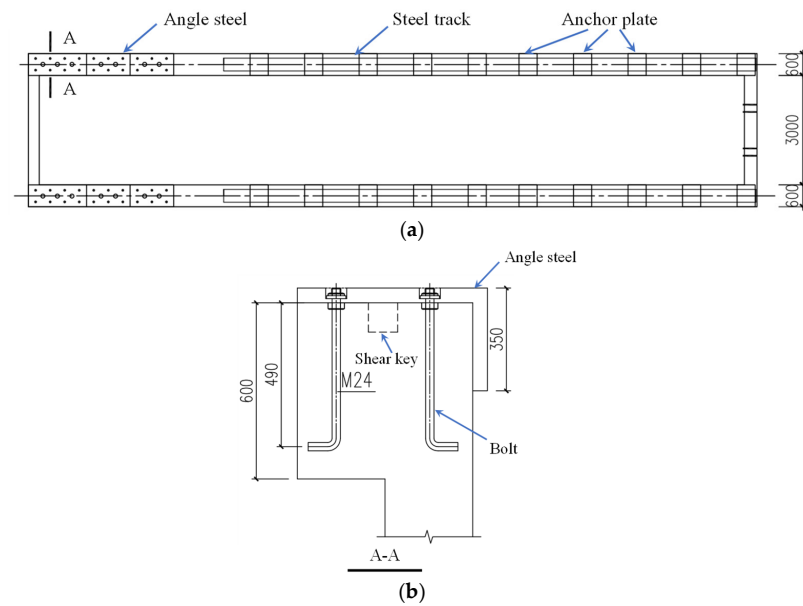


Figure 3. Plan view of the soil tank (a) arrangement of angle steels and steel tracks and (b) connection between steel angle and soil tank.

2.3. Loading System

The loading system comprises a supporting frame, a cross-sliding frame, a displacement loading system, a bending moment loading system, an elastic support, and the hydraulic power units and control system. The first four systems were assembled to apply the excitations to the SCR, as shown in Figure 4. The cross-sliding frame was fixed to the supporting frame, and its lateral movement was driven by the lateral hydraulic jack that was fixed on one side of the supporting frame. The vertical movement of the SCR was realized by the vertical hydraulic jack fastened to the top of the cross-sliding frame. The piston rod of this vertical jack was connected to the top of the bending moment loading system. A flange was installed at the front of the bending moment loading system to connect the model SCR. The bottoms of two axial hydraulic jacks were fixed on the angle steels of the soil tank, and the piston rods were connected to the supporting frame to adjust its axial position. The loading system was activated and controlled by the hydraulic power units and control system. The tail end of SCR was connected to the elastic support which is fixed to the wall of the soil tank.

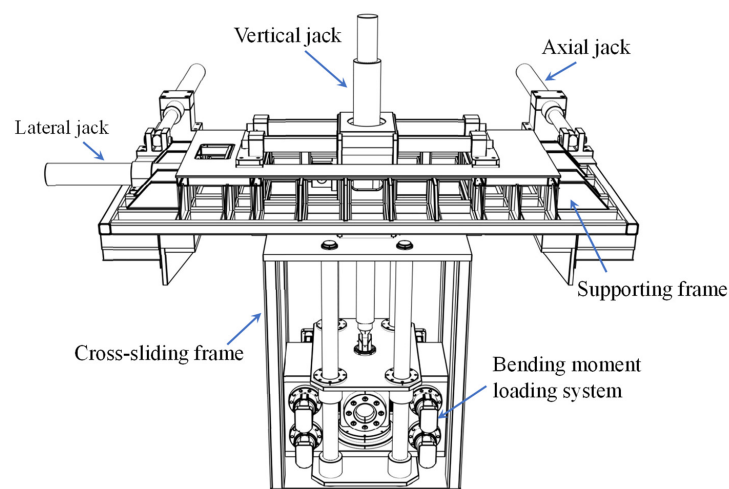


Figure 4. Assembly of the supporting frame, cross-sliding frame, and displacement and bending moment loading systems.

2.3.1. Supporting Frame

The supporting frame was constructed by welding the steel plates and steel box beams together. The three-dimensional illustration of the frame is shown in Figure 5. The purpose of this frame is to sustain the weight of the whole loading facility and the reaction force during the test. Instead of using thick steel plates, the adoption of steel box beams could reduce the self-weight and increase the flexural rigidity. Stiffeners were arranged around each side of the frame to further increase the rigidity. Since the frame should avoid any movement during the test, the electromagnets were activated to link the supporting frame and the angle steel on the soil tank.

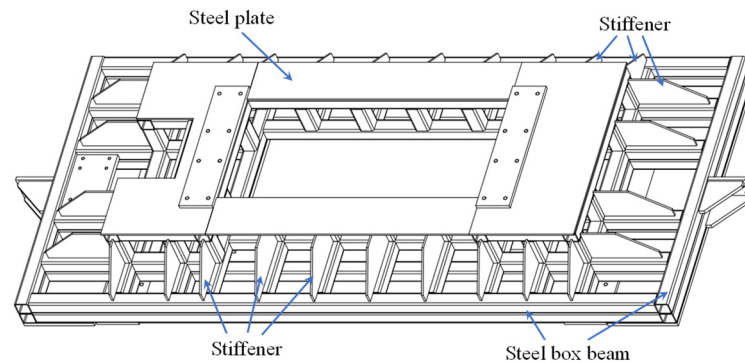


Figure 5. Schematic of the supporting frame.

2.3.2. Cross-Sliding Frame

The cross-sliding frame can accommodate the in-plane movement of the loading end of SCR. Its structure can be decomposed into the upper frame and the lower frame, as shown in Figure 6. In the upper frame, four steel rods were fastened to the supporting frame, and a sliding block was driven to slide along the rods through the lateral hydraulic jack. The vertical hydraulic jack was fixed to this sliding block. The steel plate at the top of the lower frame was also welded to the bottom of the box-shaped sliding block, and therefore, the central line of the vertical hydraulic jack would always coincide with that of the lower frame. The lower frame constituted two steel plates and four steel box columns, exhibiting the advantages of lighter self-weight and higher bending rigidity. Four steel rods were arranged within the columns as the guide of the bending moment loading system. Meanwhile, the rods also contributed to increasing the flexural rigidity of the lower frame.

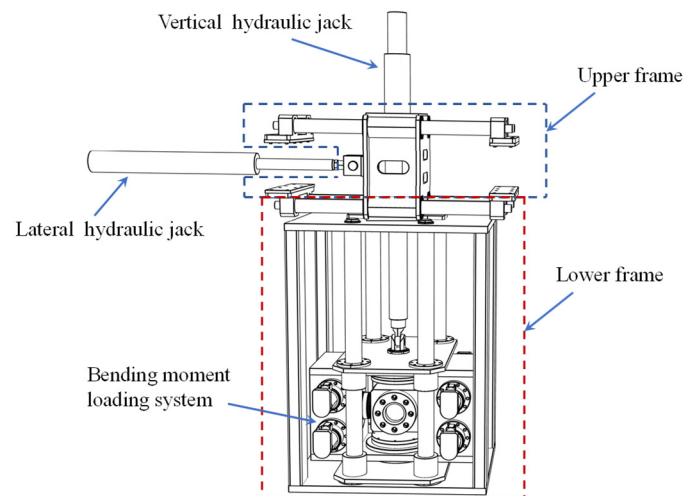


Figure 6. Schematic of the cross-sliding frame.

2.3.3. Displacement Loading System

The displacement loading system is composed of axial, lateral, and vertical hydraulic jacks. The structure of the vertical loading jack is shown in Figure 7 as an example. Since the purpose of the axial jacks was to locate the supporting frame, only low-speed displacement was allowed, whereas the other jacks could realize high-speed cyclic loading. The strokes of the axial, lateral, and vertical jacks were 960 mm, 1010 mm, and 1200 mm, respectively. For the in situ deep-water SCR, the period of short-term heave motion and sway motion is concentrated within 5~12 s. If the lowest period is reached, the moving range of the truncated point of SCR is small. The highest loading frequency of the jacks was 0.5 Hz when the loading amplitude was 100 mm, and 0.17 Hz when the loading amplitude was 300 mm. Therefore, the loading capacity of the hydraulic jacks can fulfill the aim of reproducing the moving condition of an in situ SCR.

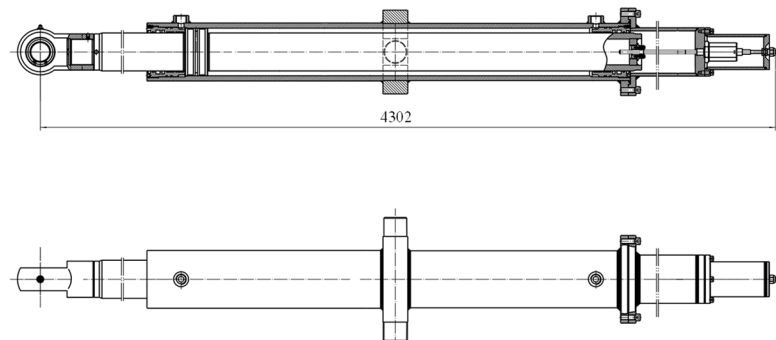


Figure 7. Structure of the vertical loading jack.

2.3.4. Bending Moment Loading System

To provide the bending moment to the loading end of SCR, two gear-rack swing hydraulic cylinders were assembled to form the bending moment loading system, as shown in Figure 8. The top and bottom of the chambers were connected through steel plates, and both output axes of the cylinders were aligned to rotate the flange simultaneously. The three-dimensional view and profile of the hydraulic cylinder are shown in Figure 9. For each cylinder, the maximum rotating angle was $\pm 15^\circ$ and the rated operating pressure was 21 MPa. Under this pressure, the output torque was 22.3 kN·m. Therefore, the total bending moment that could be provided to the SCR was 44.6 kN·m during the configuration-building stage. During the cyclic loading stage, the bending moment should be calculated through the stress analysis of the SCR rather than the sensor, because the rotating angle is restricted.

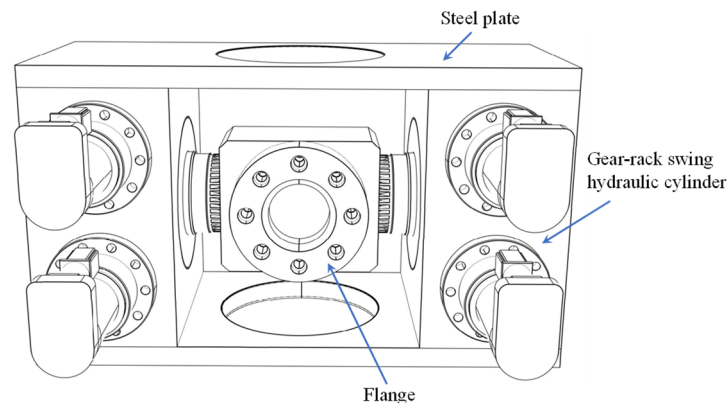


Figure 8. Schematic of the bending moment loading system.

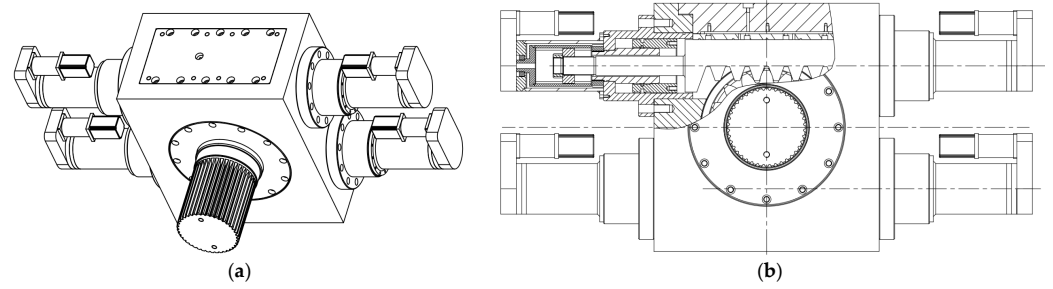


Figure 9. Structure of the gear-rack swing hydraulic cylinder: (a) three-dimensional view and (b) profile.

2.3.5. Hydraulic Power Units and Control System

The hydraulic power units contain four electric motors with a rated power of 22 kW, one electric motor of 11 kW, four hydraulic pumps, an air-cooling system, a fuel tank, and auxiliary equipment including piezometers and valves. The assembly is shown in Figure 10. The operating pressure of this system is 20 MPa, and the rate of flow is 120 L/min. To control the loading system through the electrical signal, electrohydraulic servo valves were integrated into the system. A shelf was constructed to accommodate the proportional valves, accumulators, filters, and an electrical control cabinet, as shown in Figure 11.

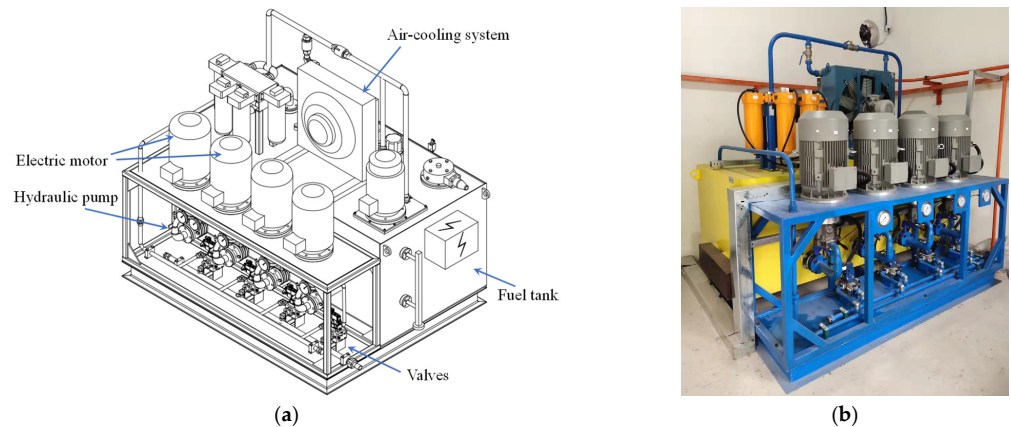


Figure 10. The hydraulic power units: (a) schematic illustration and (b) constructed assembly.



Figure 11. Assembly of the electrohydraulic servo valves and electrical control cabinet.

2.3.6. Elastic Support

The elastic support is used to simulate the constraint effect of the flowline part of the riser to the model SCR. The structure can be decomposed into two fixed supports and one movable support, as shown in Figure 12. The fixed supports were anchored to the wall of the soil tank using high-strength bolts. For each fixed support, two steel rods were arranged as the guides of the movable support. A steel plate with circular openings could slide vertically along the rods, and its movement was restricted by the vertical springs. The front steel plate of moveable support was welded perpendicularly to the sliding steel plates and could only move vertically, whereas the back steel plate shared the same vertical position with the front one, and could move axially along four steel rods. The axial stiffness was provided by two axial springs, with one end fixed to the front plate and the other fixed to the back plate. All the springs in this elastic support are changeable, allowing the stiffness to be varied according to the requirement of the test. In this study, the vertical stiffness was set to a large value to avoid the maximum penetration of SCR concentrating within this area, whereas the axial stiffness was much lower, allowing the axial movement of SCR to avoid extremely large axial force during the cyclic displacement excitations. The flange was connected to the back plate of the movable support via a spherical hinge. Therefore, the SCR could rotate freely at this end, and the bending moment could be released.

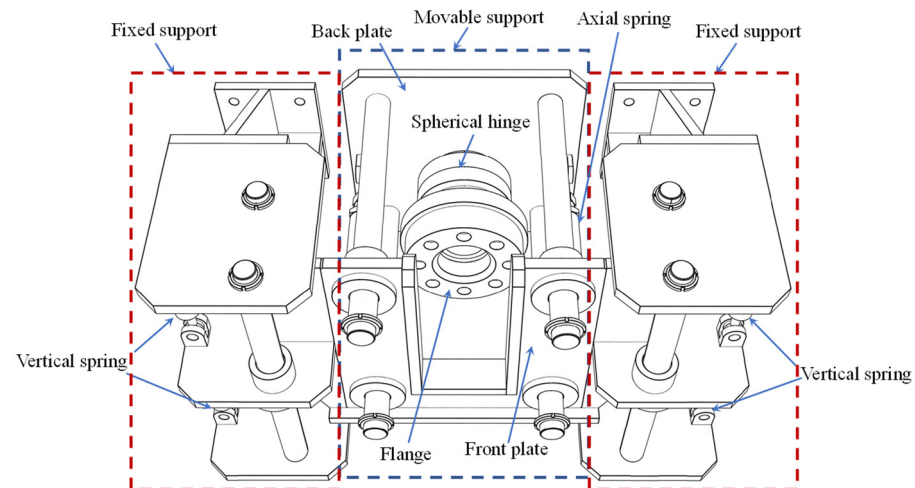


Figure 12. Schematic of the elastic support.

2.4. Soil Stirring System

The properties of the test soil can significantly affect the mechanical behavior of the model SCR. Clayey soil with an undrained shear strength similar to that in deep water should be prepared. Uniformity is another key indicator that should be guaranteed for such a large amount of soil. The clay can be prepared using kaolin clay powder, for its properties similar to the subsea soil, or by collecting near-shore or in situ soil. Since there will be some impurities in the collected soil, the clay should be dried and sieved to obtain the pure clay powder. It is hard to fully saturate the clay after adding enough water and waiting for a long period, owing to its low permeability. To solve these problems, a soil stirring system was proposed. The soil powder was divided into several portions to be dropped into the soil tank. After adding each portion, the water was poured into the tank, and the stirring system was used to mix the content. When all the soil and water were thrown into the tank, the stirrer was forced to move vertically, while the frame would slide along the track on the soil tank simultaneously. This allowed all the clay to be stirred and mixed thoroughly to obtain the homogeneous test soil. Then, the soil could settle under its self-weight to be consolidated, or the vacuum preloading method could be used to accelerate the process, as shown in Figure 13. After the soil was fully saturated and consolidated, the surface was scraped using the stirring system to guarantee the planeness.

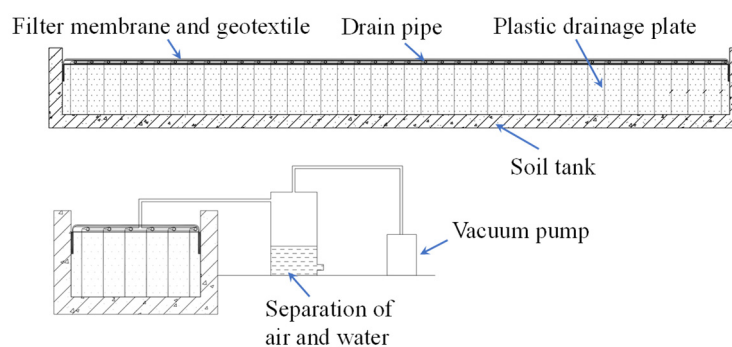


Figure 13. Vacuum preloading system.

The soil stirring system contains a portal frame, a power system, a changeable stirrer, and a scraper, as shown in Figure 14. The portal frame can travel along the track of the soil tank, whereas the vertical track can move horizontally along the lateral track that was fastened on the frame. Four electric motors were used in this system. The first one was to control the movement of the portal frame, the second one was fixed to the vertical track to drive its lateral movement, the third one was connected to the stirring shaft to control its vertical position, and the last one was installed on the top of the shaft to rotate the shaft and stirrer. The stirrer can be changed according to the property of the test soil. The scraper was adopted to guarantee the planeness of the clay, and its vertical position can also be adjusted to fit different targets of soil depth. The scraper is also detachable. Therefore, when the stirrer or the scraper was working, the other was removed to avoid interference.

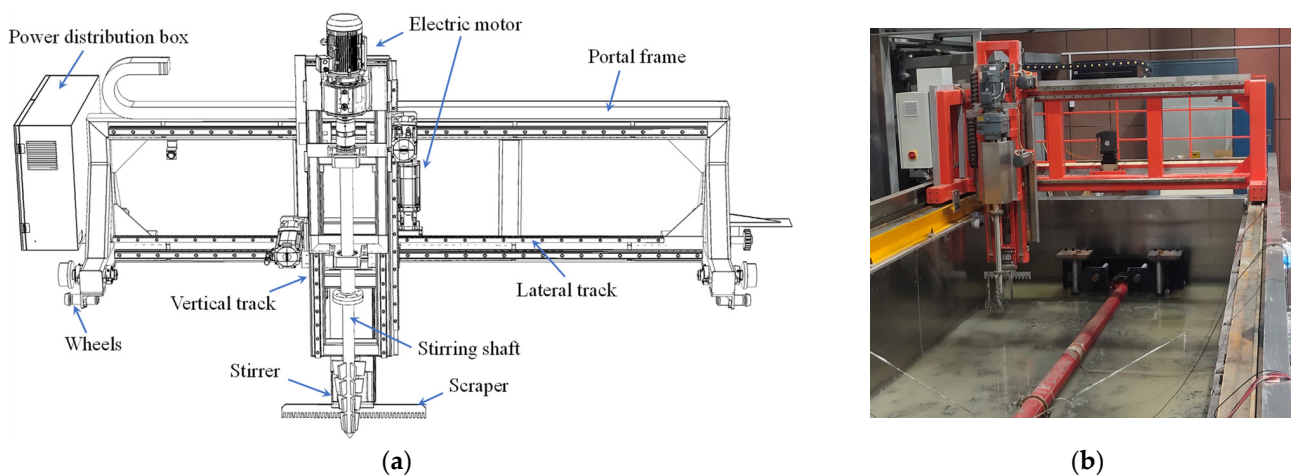


Figure 14. The soil stirring system: (a) schematic illustration and (b) constructed assembly.

3. Experiment Setup and Procedures

3.1. Determination of Experimental Parameters

To determine the parameters in the model test, a numerical model of in situ SCR was built using the vector form intrinsic finite element method (VFIFE), which is suitable to solve high-nonlinear problems. Similar to the lumped mass method adopted in the commercial software OrcaFlex, the riser was also replaced by a series of mass points. A beam element was used to connect each pair of adjacent points to transmit the internal force and provide stiffness. The position of the points represented the configuration of SCR, whereas the points' movements under the imbalanced forces were used to model the vibration of the riser. One of the major differences between the lumped mass method and the VFIFE method is that the deformations of the beam elements are calculated based on the virtual reverse motion for the VFIFE method. Detailed descriptions of the VFIFE method can be referred to in [1]. The nonlinear vertical soil model proposed by Randolph and Quiggin [6] was also integrated into this finite element model.

The prototype SCR used in this study has been put into production in the Lingshui project in China. The SCR is 2130 m long, with an outer diameter of 168 mm and a thickness of 18.3 mm. The seabed is clayey soil with an undrained shear strength of 4–8 kPa. Each end of the SCR was modeled as hinged in the numerical model. Detailed parameters used in the model are listed in Table 1. The static configuration of SCR was established under the submerged weight and soil resistance, as shown in Figure 15. The static in-plane bending moment was concentrated within the catenary part near the TDP as shown in Figure 16, with a maximum value of 17.47 kN·m. The distribution of seabed resistance and the developed seabed trench profile are shown in Figure 17. The resistance kept increasing within the trench mouth, and reached its peak value at the deepest point of the trench. Subsequently, the resistance decreased slightly along the trench tail and stabilized at the value that equaled the submerged self-weight of SCR.

Table 1. Detailed parameters used in the model.

Properties of Riser and Seabed	Value	Unit
Total length L	2130.0	m
External diameter D	168.0	mm
Wall thickness t	18.3	mm
Mudline shear strength s_{um}	6.0	kPa
Shear strength gradient k	1.5	kPa/m
Power law parameter a	6.0	
Power law parameter b	0.25	
Normalized maximum stiffness K_{max}	200	
Suction ratio f_{suc}	0.2	
Normalized suction decay distance λ_{suc}	0.5	
Normalized repenetration offset after uplift λ_{rep}	0.5	
Saturated soil density ρ_s	1500.0	kg/m ³
Soil buoyancy factor f_b	1.5	

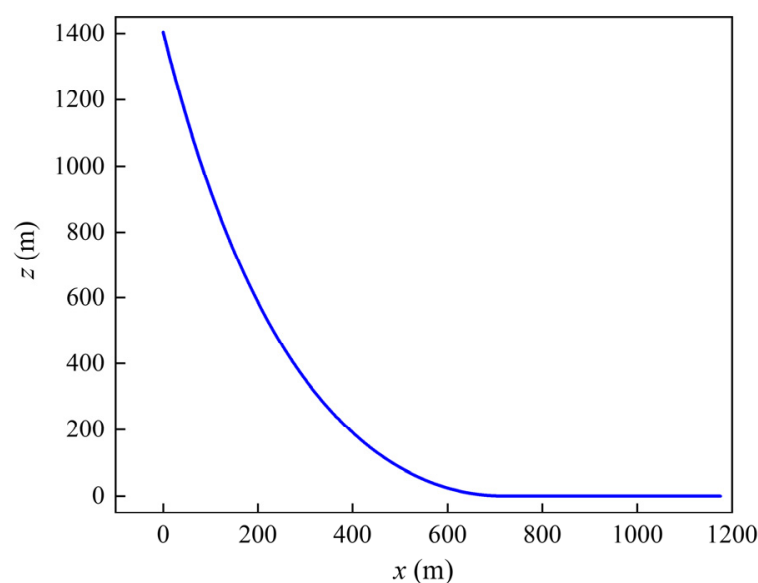


Figure 15. Static configuration of in situ SCR.

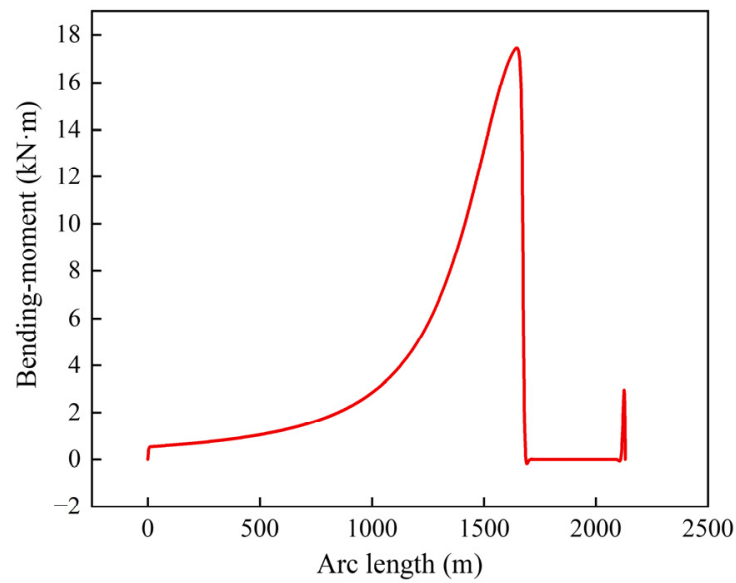


Figure 16. Distribution of bending moment.

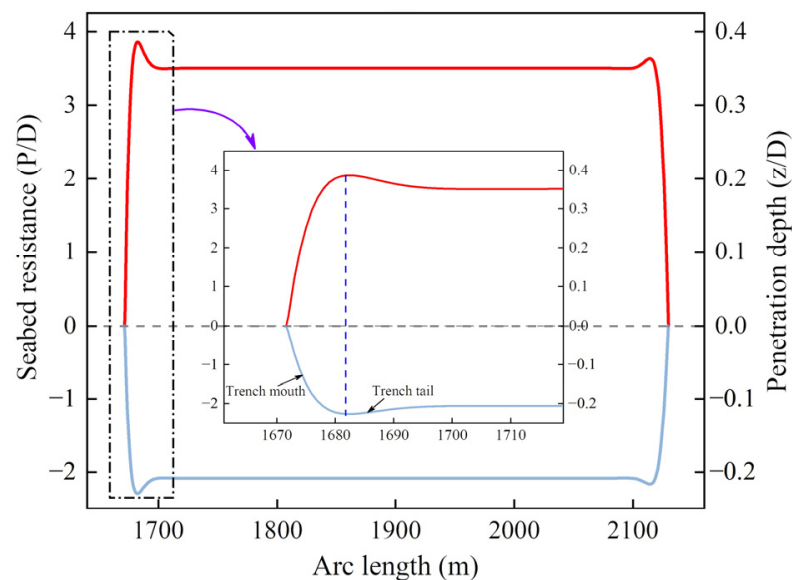


Figure 17. Distribution of seabed resistance and developed seabed trench.

A reference point P at the arc length of 1660.0 m was taken as the truncated point in the model test. The vertical clearance between point P and the seabed was 0.3 m when the static configuration of SCR was established. After applying a harmonic heave motion with an amplitude of 1.0 m and a period of 15 s, the time history of the vertical displacement of point P was obtained, as shown in Figure 18. It proves that harmonic sine-wave motions are suitable to be applied to the truncated point of the model SCR. The relationship between the displacement ranges of the top end and point P is shown in Figure 19. When the heave motion reached an amplitude of 1.5 m, the moving range of point P was 0.72 m. Therefore, the applied displacement to the truncated point lay within the capability of the vertical hydraulic loading jack. Similarly, the horizontal moving range of point P was also less than the maximum displacement of the horizontal hydraulic loading jack.

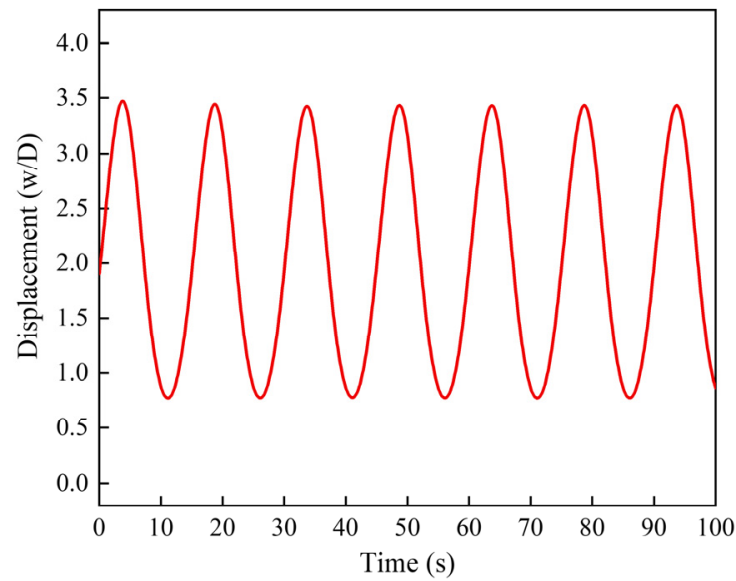


Figure 18. Displacement oscillation history of point P.

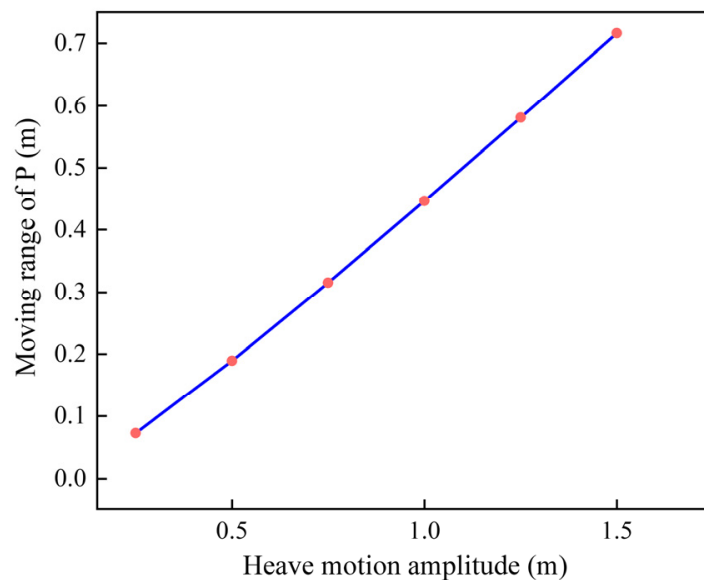


Figure 19. Relationship between heave motion amplitude and moving range of P.

In the model test of the SCR, a steel pipe with a diameter of 168 mm was adopted, similar to the in situ SCR. The wall thickness was reduced to 8 mm to magnify the deformation under the submerged weight and bending moment, since the length of the model SCR was 17.0 m. When the riser developed its configuration, the bending moment applied to the truncated point P was within the capacity of the bending moment loading system. The cyclic vertical and lateral displacement loads can be applied to the loading point of model SCR individually or simultaneously, with their amplitudes similar to the moving ranges of point P of the prototype SCR. The variation in the position of the loading end made the bending moment provided by the loading system unrealistic to precisely control during the loading stage. Therefore, the angle of the riser at the loading end was fixed, and remained constant once the static configuration of the SCR was established. It also helped to determine the boundary condition of the SCR in the numerical model. Although the stress variation may have some differences compared with that of the in situ riser, this method would not obstruct the oscillation of SCR and the interaction between the riser and seabed. Since the major target of this test is to study the influence of the riser–soil

interaction on the mechanical behavior of SCR and verify the feasibility of the numerical soil model, the simplifications were deemed acceptable.

3.2. Layout of Instrumentation

To track the stress variation and determine the bending moment and axial tension distribution, 9 sets of strain gauges were arranged along the model SCR, as shown in Figure 20. For each set, four strain gauges were pasted on the same section of the pipe with an interval of 90°. Since the steel pipe remained elastic throughout the experiment, the stress can be obtained through the strain value. The tension and bending moment at each section can be determined according to Equations (1) and (2), respectively.

$$T = \sigma_{ave}A \tag{1}$$

$$M = \frac{\Delta\sigma}{D_{out}} I_z \tag{2}$$

where T is the axial force, σ_{ave} is the average value of the stresses within the section, A is the area of the cross section, $\Delta\sigma$ is the difference value of the stresses that coincides with the direction of the moment, D_{out} is the outer diameter of the pipe, and I_z is the inertia moment.

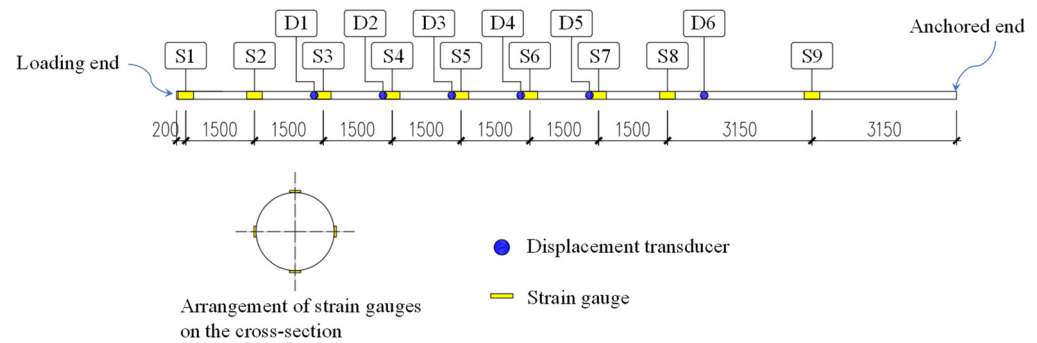


Figure 20. Arrangement of strain gauges and displacement transducers.

To obtain the displacement of the model SCR, 6 groups of draw wire displacement transducers were attached to the pipe, as shown in Figure 21. Since the riser would have in-plane and out-of-plane vibrations, the vertical and lateral movement should be recorded, respectively. Therefore, two displacement sensors were arranged diagonally in each group to realize this, as shown in Figure 22, and the horizontal and vertical displacement components could be calculated based on Equations (3) and (4), respectively.

$$\Delta H = \frac{L_1'^2 - L_2'^2}{2L_H} \tag{3}$$

$$\Delta V = \sqrt{L_1'^2 - \left(\frac{L_H^2 + L_1'^2 - L_2'^2}{2L_H} \right)^2} - L_V \tag{4}$$

where ΔH and ΔV are the vertical and horizontal displacement components, respectively, L_1' and L_2' are the displaced distance between each transducer and the model SCR, L_H is the horizontal distance between the transducers, and L_V is the vertical clearance between the transducers and the middle of the section of model SCR at the beginning of the test, and can be calculated as $L_V = \sqrt{L_1^2 - \frac{L_H^2}{2}}$, where L_1 is the initial distance between the transducer and the section of SCR. The same vertical elevations of the displacement transducers should be guaranteed when they were arranged. Since the model SCR was initially situated along the central line of the soil tank, the horizontal distances between the model SCR and each transducer in one group were the same.

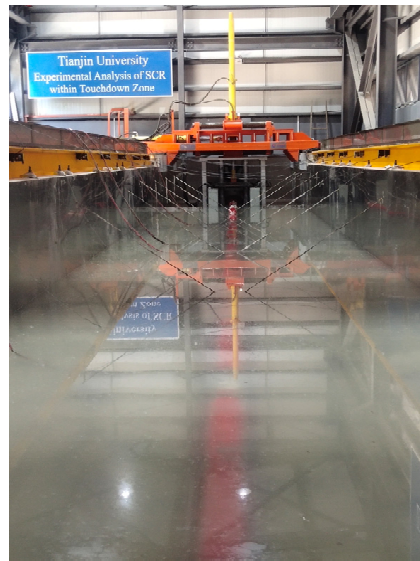


Figure 21. Installation of displacement transducers.

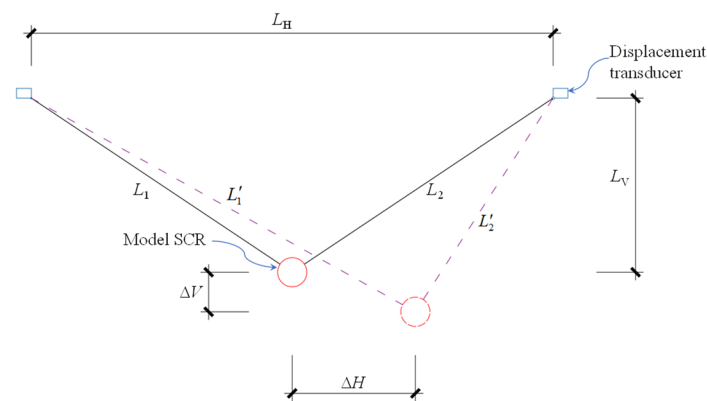


Figure 22. Calculation of the vertical and horizontal displacement.

3.3. Test Procedures

Before the experiment, the test clayey soil was prepared with the help of the soil stirring system and then consolidated via the vacuum preloading method. The undrained shear strength of the soil was obtained by the vane shear test, and its value was 6 kPa. The supporting frame was adjusted axially to make sure that the flanges of the model SCR could be connected to the bending moment loading system and the elastic support, respectively. Enough water was poured into the soil tank to ensure that the riser was submerged. The test of model SCR can be divided into three loading procedures. In the first procedure, the vertical position of the flange middle of the loading end was uplifted 300 mm above that of the hinged end, and the water was injected into the pipe to increase its self-weight. Since the wall thickness of the model SCR was decreased, the applied bending moment should be reduced according to the decrement of the section moment of inertia, allowing the stress of model SCR to be similar to that of the in situ SCR. Therefore, the bending moment of 9.2 kN·m was applied to this end. When the variation of displacement recorded by the transducers was less than 1mm, the static configuration of the model SCR was established.

Subsequently, the cyclic vertical displacements were applied to the truncated point of model SCR in the second loading stage. Different loading amplitudes and periods were selected to investigate their influences on the mechanical behavior of the SCR. The loading sequence was also an important parameter, because a severer motion would induce a deeper trench and may affect the stress distribution of SCR. The loading conditions are listed in Table 2.

Table 2. Cyclic loading conditions.

Loading Sequence	Loading Direction	Amplitude (m)	Period (s)
1	Vertical	0.1	20
2		0.2	20, 15, 10
3		0.3	20, 15, 10
4		0.2	15
5	Horizontal	0.1	15
6		0.2	15

The cyclic horizontal displacements were applied in the third stage. Although the vertical oscillation of SCR is the main factor that induces fatigue damage, the horizontal movement of SCR within the TDZ also widens the trench and affects the mechanical performance of the riser. Therefore, different amplitudes of the sway motions were considered in this test. After this stage, the water in the soil tank was also pumped out to observe the developed trench shape.

4. Experiment Results and Analysis

4.1. Static Loading Stage and Numerical Comparison

Since the riser will experience dynamic oscillations during the installation process, the seabed soil will be disturbed and the riser segments will penetrate deeper than that under its submerged weight. The overpenetration of the riser will induce larger seabed resistance when the riser oscillates laterally. To consider this effect, the model riser was placed horizontally on the seabed surface before the soil preparation process and lowered to produce a shallow trench. After the soil was fully consolidated, the distance between the seabed surface and the trench bottom was 105 mm.

After the position of the loading point was situated 0.3 m above the elastic supporting end and the bending moment was applied, the model SCR developed its configuration, as shown in Figure 23. The angle of the riser at the tail end was nonzero, because the rigidity of this steel model SCR was larger than those of the PE and PVC pipes used in the literature. The simulated configuration of the model SCR using the VFIFE method was similar to the test result, proving the correctness of the model. The distribution of the bending moment is shown in Figure 24, and high similarities exhibit the accuracy of the strain data gathered by the strain gauges. The bending moment increased gradually from the loading end and reached its peak at 7.0 m. After reaching the maximum value, the bending moment decreased to zero when approaching the tail end.

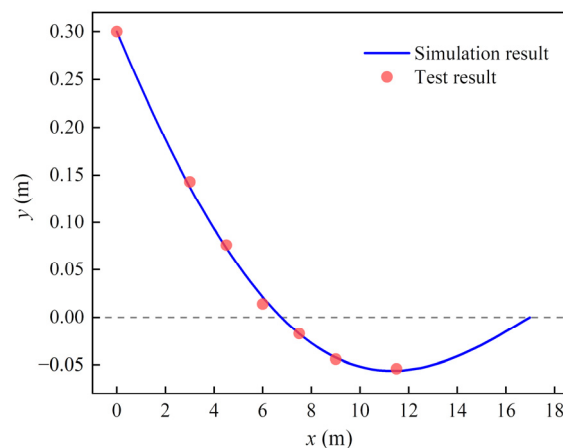


Figure 23. Static configuration of the model SCR.

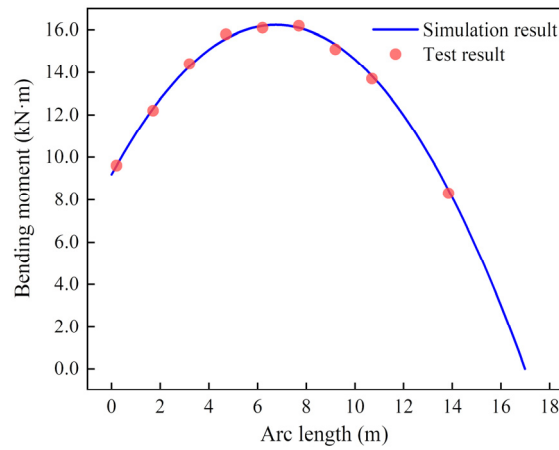
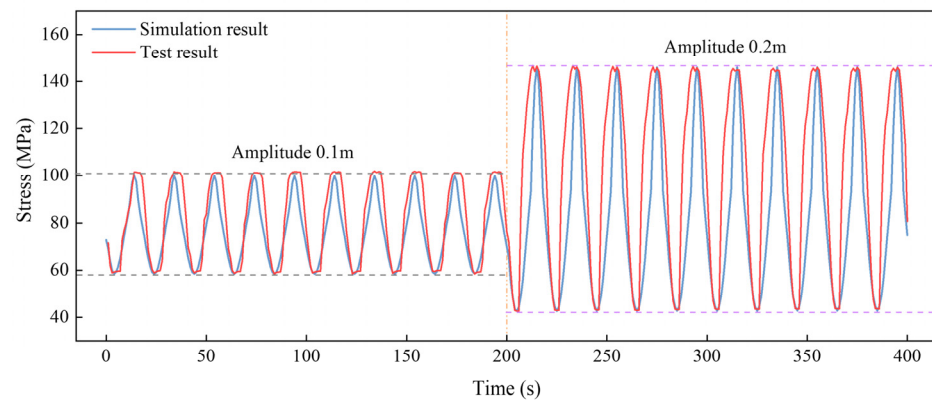


Figure 24. Distribution of bending moment of the model SCR.

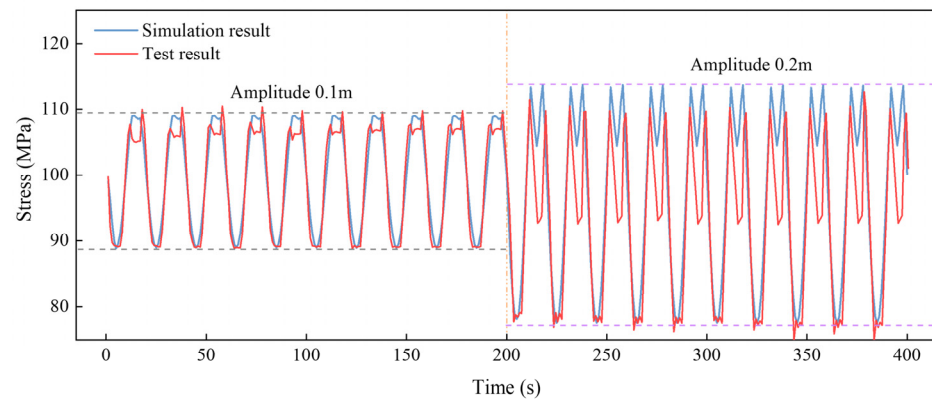
4.2. Cyclic Vertical Displacement Loading

4.2.1. Effect of Increasing Loading Amplitude

The cyclic vertical displacement load with an amplitude of 100 mm and a period of 20 s was first applied to the model SCR. After several cycles, the loading amplitude increased to 200 mm while keeping the period constant. The time history of the in-plane stress values (half of the difference value of the stress obtained by the strain gauges at the bottom and top of a cross section) at points S2, S5, and S8 are shown in Figure 25. For S2, the stress variation curve is similar to a sinusoid. Once the loading end was uplifted, the stress value decreased gradually and approached the minimum.



(a)



(b)

Figure 25. Cont.

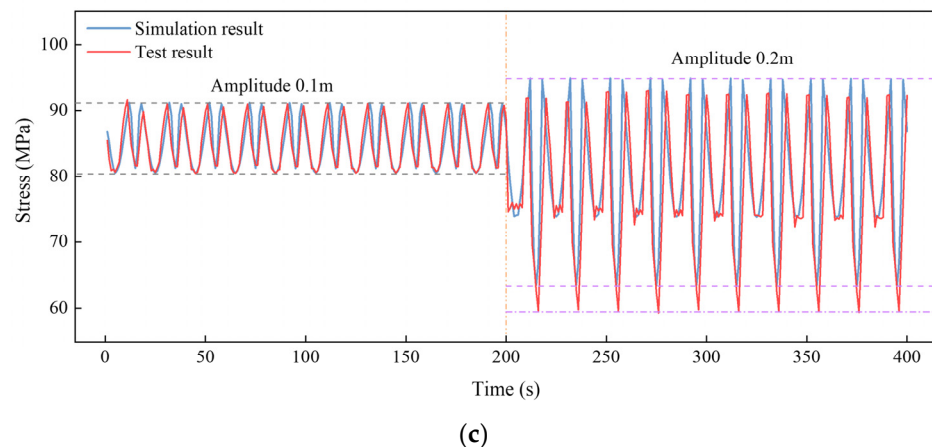


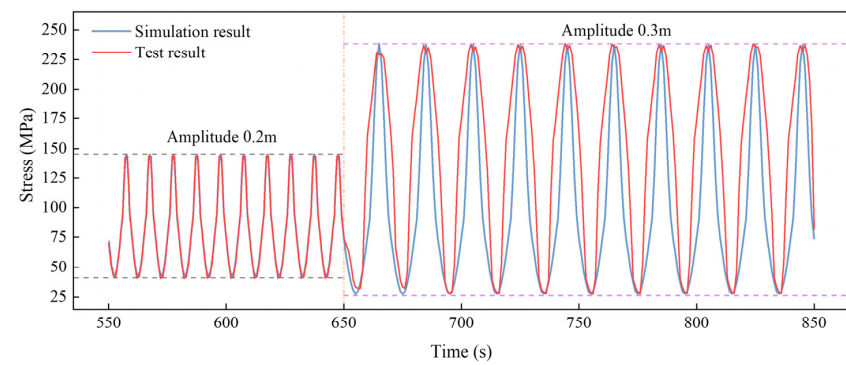
Figure 25. Time histories of the in-plane stress when the amplitude increased from 100 mm to 200 mm: (a) S2; (b) S5; and (c) S8.

Regarding S5 and S8, the time history curves of in-plane stress were no longer sinusoids, as shown in Figure 25b,c. The stress decreased when the truncated point of the model SCR approached the upper end, and vice versa. The riser segment within the middle of the SCR began to penetrate the seabed when the riser was lowered. The stress value apparently decreased during the riser penetration, since the seabed resistance became larger than the submerged weight of the riser and decreased the bending moment at the middle of the SCR. The decrease in stress was more significant for S8 than for S5. Subsequently, the riser was uplifted, and the stress increased and reached the second peak value as the seabed resistance was released. This second peak value may have been larger than the first peak because the clay seabed could provide the suction force when the riser segment began to uplift. This phenomenon was captured by both of the experiment and numerical simulation. The minimum value of stress was reached when the riser was uplifted to the top position for S5, whereas the minimum stress of S8 occurred when the SCR was lowered and a larger seabed resistance was activated. Furthermore, the variation in the minimum stress was more noticeable than the variation in the maximum stress. The stress range increased by 139.9%, 74.0%, and 203.4% for S2, S5, and S8, respectively, when the displacement amplitude increased from 100 mm to 200 mm.

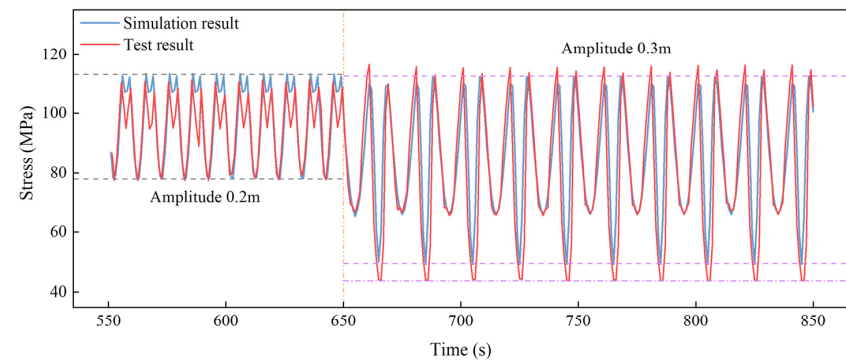
The variations of time history curves of the in-plane stress exhibit similar trends when the loading amplitude increased from 200 mm to 300 mm, as shown in Figure 26. The stress range increased by 104.6%, 114.3%, and 63.6% for S2, S5, and S8, respectively. It should be mentioned that when the loading amplitude increased to 300 mm, the minimum stress of S5 was reached as the riser was lowered and penetrated deeper into the seabed.

4.2.2. Effect of Increasing the Loading Frequency

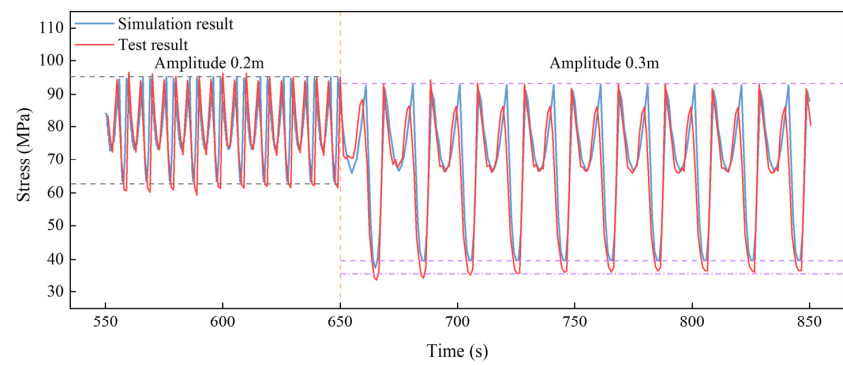
Three periods of 20 s, 15 s, and 10 s were chosen to study the influence of the loading frequency. The time history curves of stress at points S2, S5, and S8 under different loading periods are drawn in Figures 27 and 28, when the loading amplitudes were 200 mm and 300 mm, respectively. Although different loading periods were selected, the maximum and minimum stresses did not exhibit significant differences, and the trends of stress variation within different loading cycles were similar. The maximum difference in the stress ranges under different loading frequencies was less than 5%. This is attributed to the fact that the total length of the truncated model SCR is less than the in situ one, and therefore, the dynamic effect is not significantly affected by the loading period. However, for the in situ SCR, a higher loading frequency will induce a severer stress variation and larger fatigue damage, since the dynamic effect is more significant.



(a)

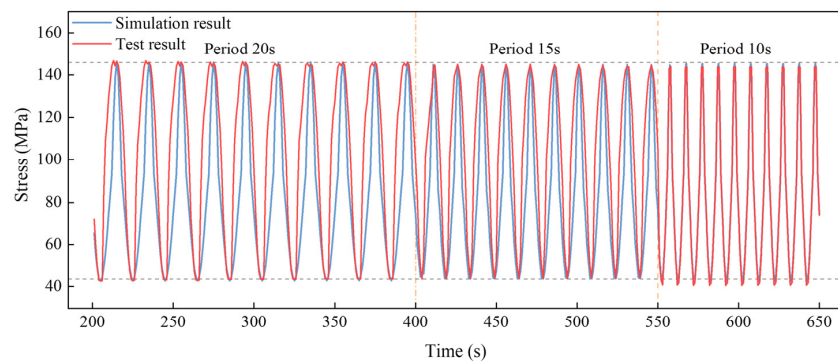


(b)



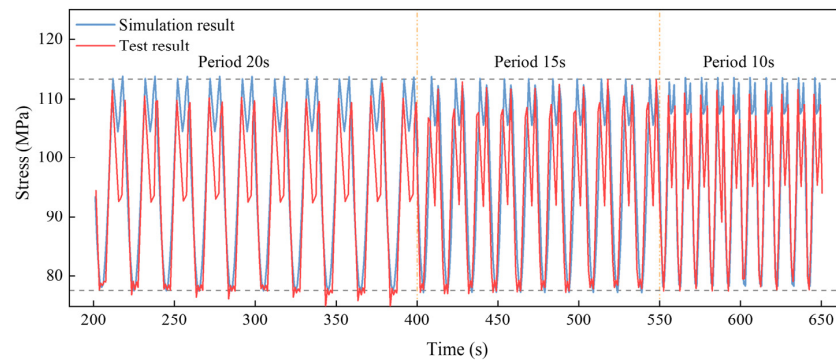
(c)

Figure 26. Time histories of the in-plane stress when the amplitude increased from 200 mm to 300 mm: (a) S2; (b) S5 and (c) S8.

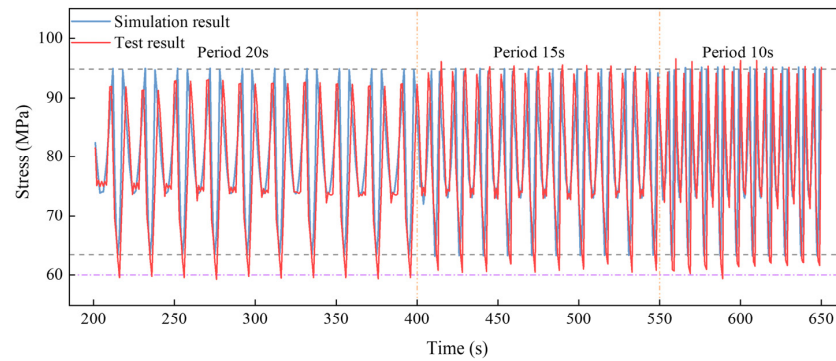


(a)

Figure 27. Cont.



(b)

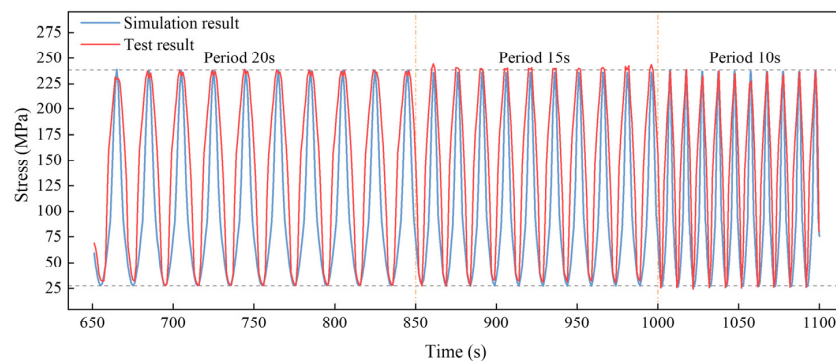


(c)

Figure 27. Time histories of the in-plane stress when the amplitude was 200 mm and the period decreased from 20 s to 10 s: (a) S2; (b) S5 and (c) S8.

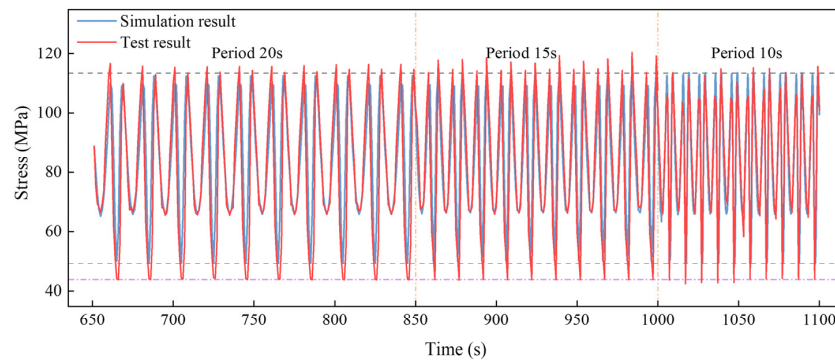
4.2.3. Effect of Decreasing the Loading Amplitude

The loading amplitude decreased from 300 mm to 200 mm after executing the above loading sequences, to determine the effects of the previous severer loading conditions on the stress variation of the model SCR. The time history curves of the in-plane stresses of S2, S5, and S8 are shown in Figure 29. When comparing the stress under 0.2 m amplitude loading with those in Figure 27, the stress range decreased by 22.4%, 3.8%, and 14.1% for S2, S5, and S8, respectively. This was caused by the deformation and degradation of seabed soil. This finding also agrees with the result drawn by Yu et al. [14] that a seabed trench helps to reduce the fatigue damage of SCR. However, since the variation of trench depth during the test was far smaller than that of an in situ trench, the decrement in stress range was not so obvious.

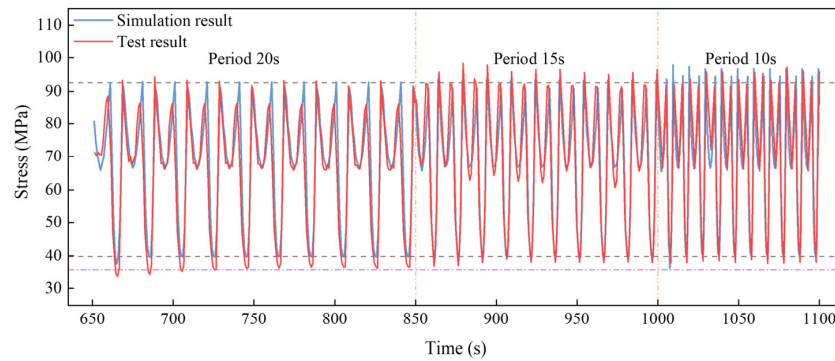


(a)

Figure 28. Cont.



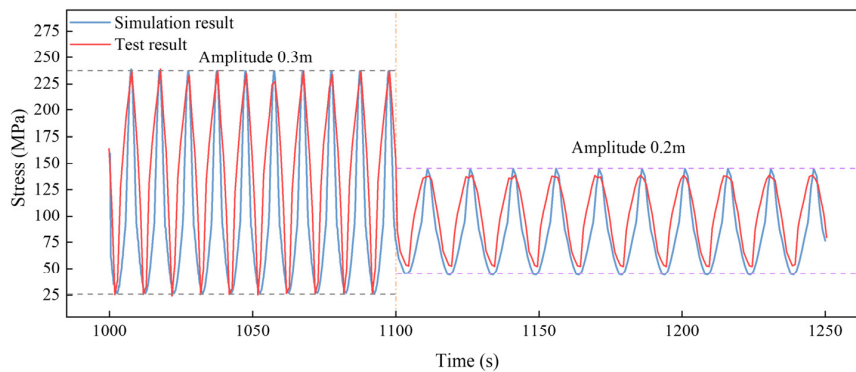
(b)



(c)

Figure 28. Time histories of the in-plane stress when the amplitude was 300 mm and the period decreased from 20 s to 10 s: (a) S2; (b) S5 and (c) S8.

Based on the comparisons in Figures 25–29, high similarities can be found between the simulation and experiment results. This proves the reliability of the nonlinear RQ soil model and the robustness of the VFIFE model. Furthermore, the variation in stress range was insignificant during a loading sequence, proving the degradation of soil was not severe. This supports the feasibility of using the nonlinear soil model without considering soil degradation, which can be simpler and own a higher safety factor. The effect of soil deformation and degradation can be substituted by the insertion of a proper predefined seabed trench, to give the lower bound of the fatigue damage of the SCR.



(a)

Figure 29. Cont.

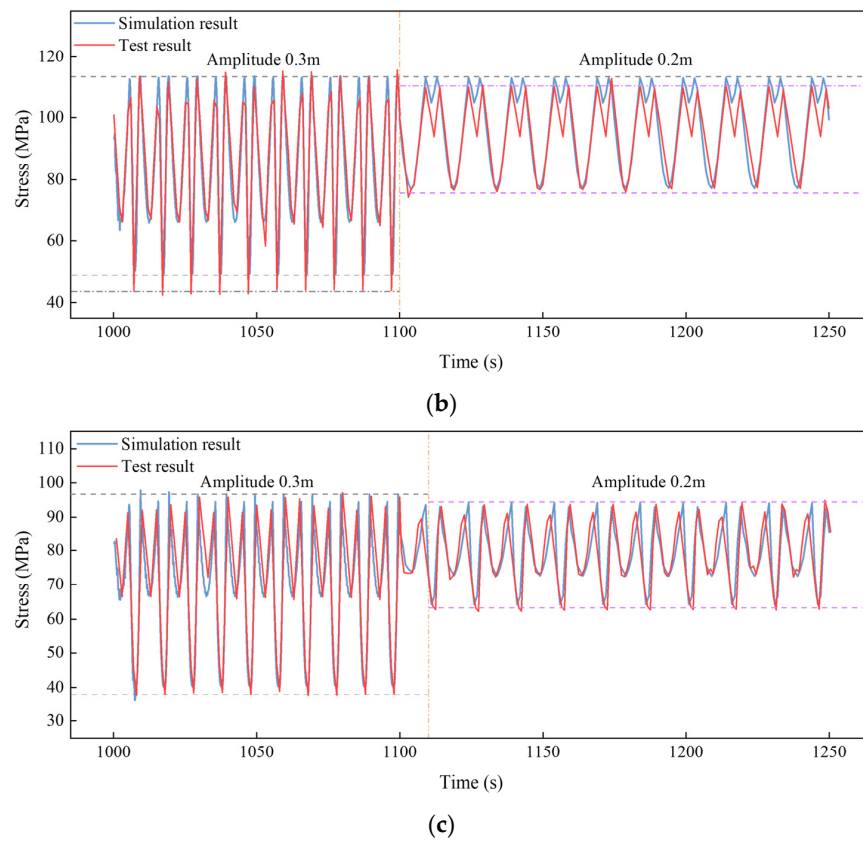


Figure 29. Time histories of the in-plane stress when the amplitude increased from 300 mm to 200 mm: (a) S2; (b) S5 and (c) S8.

4.2.4. Stress Range Analysis

Since the loading frequency would not significantly affect the stress variation, the in-plane stress range distributions along the model SCR under different loading amplitudes were analyzed. The comparisons between the test and numerical results are shown in Figure 30. The comparison between the in-plane stress ranges of the SCR under different loading amplitudes is shown in Figure 30d. When applying a severer cyclic displacement, the stress range along the whole SCR becomes larger, and the increment is more significant towards the loading end.

For the SCR with a loading amplitude of 0.1m, the stress range continued to decrease when approaching the anchored point. However, the decreasing speed has a transition point within the middle of SCR, as the slope of the curve tends to be smaller after this point. As the amplitude became larger, the stress range along the SCR began to decrease from the loading point first and then had an increment within the middle of SCR, before decreasing to zero at the anchored point. This is because the minimum stress within the middle of SCR occurred when the segment penetrated the seabed rather than uplifting to the top position. The location of the peak value of the stress range within the middle of SCR tended to move to the loading point once the loading amplitude was increased from 0.2 m to 0.3 m.

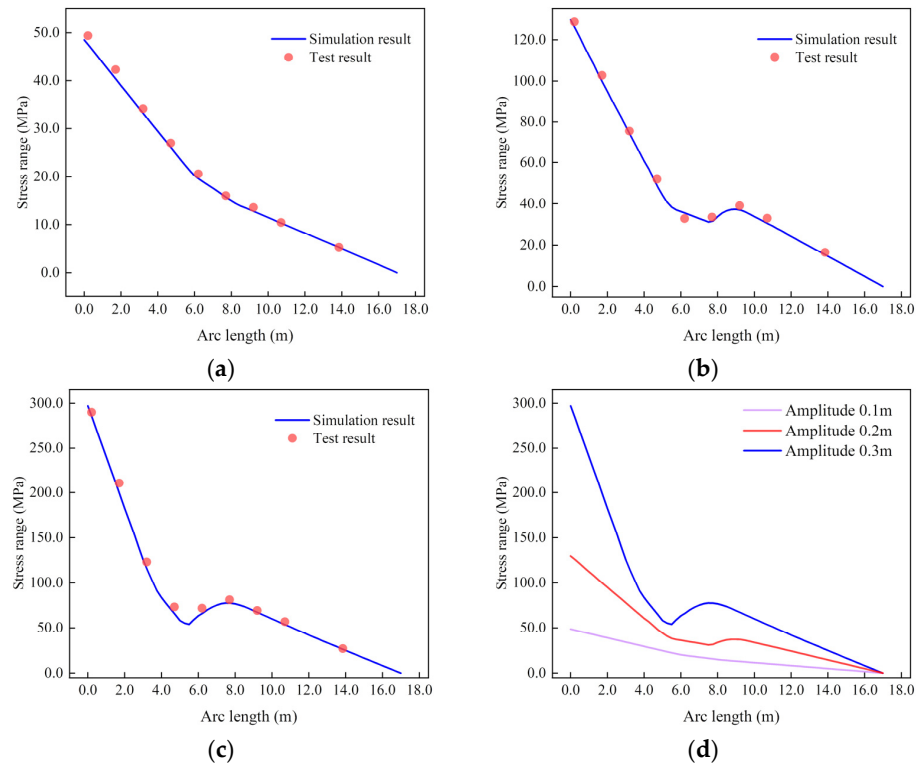


Figure 30. In-plane stress range distribution under different loading amplitudes: (a) 100 mm; (b) 200 mm; (c) 300 mm; (d) comparison of the stress ranges.

4.2.5. Seabed Trench Analysis

After executing the vertical loading sequences, the seabed was deformed under the oscillation of the model SCR. The developed trench profile can be obtained as the largest deformation of the riser during the test, and is drawn in Figure 31. A ladle-shaped trench with a maximum depth of 0.71 D was situated within the middle of SCR, and its profile was similar to that of the in situ trenches. For the centrifuge test conducted by Elliott et al. [26], although the trench shape was also similar to a ladle, its mouth was towards the anchored point. The difference in the trench directions is because the bending moment was considered in this study. This moment induced the larger deformation of the riser near the loading side, which helped to model the mechanical behavior of in situ SCR and produce a seabed trench with the correct profile.

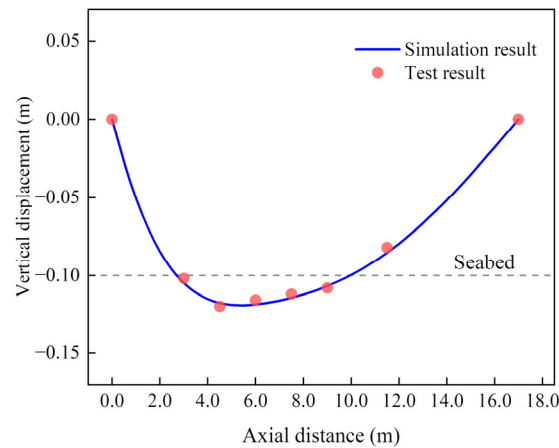


Figure 31. Developed vertical seabed trench.

4.3. Cyclic Horizontal Displacement Loading

4.3.1. Effect of Increasing Loading Amplitude

Horizontal cyclic displacement loads with amplitudes of 100 mm and 200 mm were applied to the truncated point. The vertical elevation of the loading end was adjusted to ensure that its center was 300 mm higher than the center of the tail end before the lateral loading. The loading period of 15 s was kept constant throughout this loading stage. Both the horizontal movement and the lateral seabed resistance contributed to stress variation within the model SCR. The time histories of the out-of-plane stress (half of the difference value of the stress obtained by the strain gauges at the left and right of a cross-section) at points S2, S5, and S8 are shown in Figure 32. All the curves were similar to the sinusoids, although the curve of S8 had some oscillation when the riser segment approached the initial position.

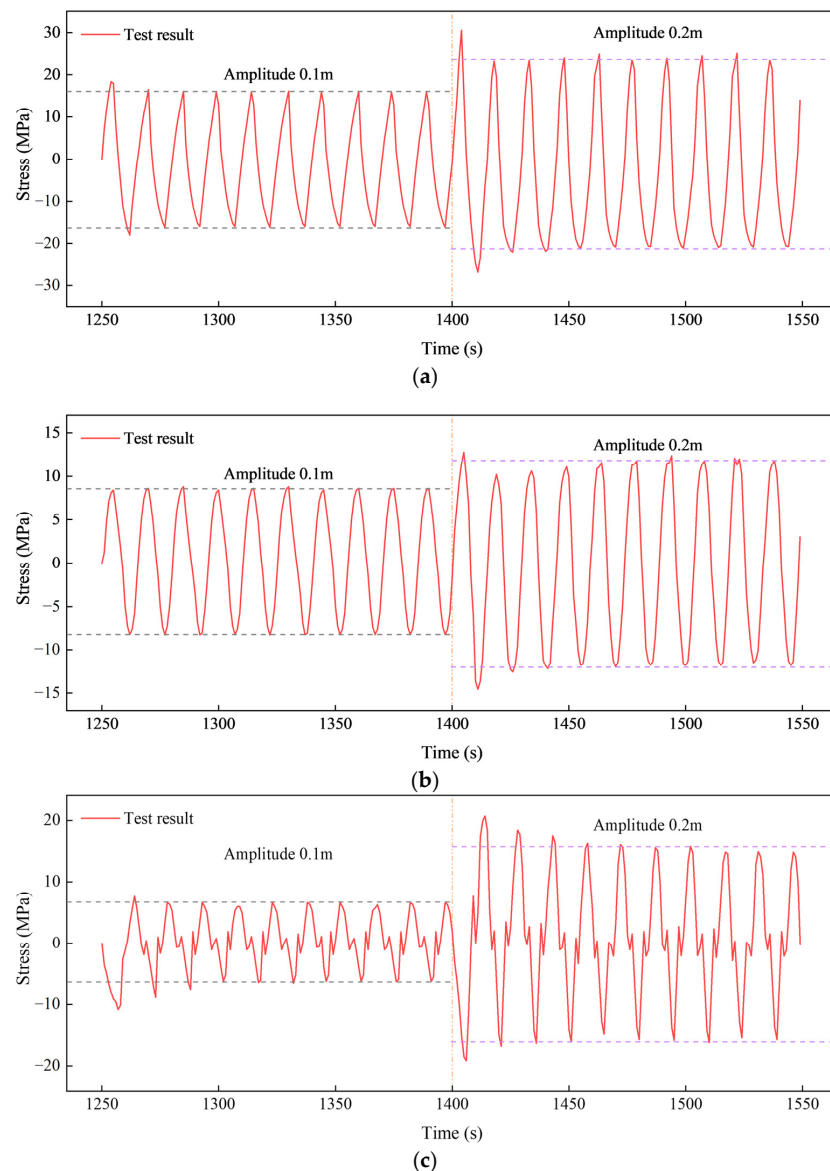


Figure 32. Time history of stress when the horizontal displacements were applied: (a) S2; (b) S5 and (c) S8.

For the first cycle of each loading amplitude, the stress range was larger than those of the following cycles, as the riser segment contacted the seabed and ploughed soil further. After this, the scraping thickness of the soil was reduced, and the lateral resistance provided

by the seabed decreased to a stable value. When the larger amplitude was applied, the stress ranges were also enlarged. It should be mentioned that the stress of point S8 had an opposite sign compared with those of S2 and S5 at any moment, i.e., when the stress of S8 was positive, the stresses of S2 and S5 was negative and vice versa. If the lateral soil resistance is not included, the sign of stress along the model SCR should be the same. Therefore, the riser-seabed resistance can change the bending moment distribution along the model SCR and have a significant influence on the mechanical behavior of the SCR.

4.3.2. Stress Range Analysis

The out-of-plane stress range distributions along the model SCR under different lateral cyclic displacements are shown in Figure 33. The stress range decreased from the loading end and reached the valley point within the middle of the SCR. Subsequently, the sign of stress would change as discussed in the previous section, and the stress range began to increase owing to the horizontal force provided by the seabed and reached a peak value. After the peak, the stress range would decrease again when approaching the hinged end.

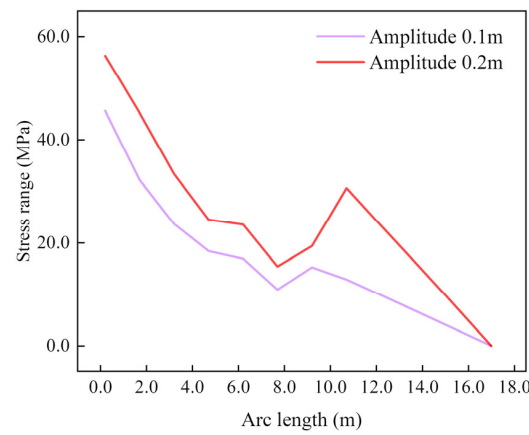


Figure 33. Out-of-plane stress range distribution along SCR.

4.3.3. Trench Plan Analysis

Considering the diameter of the riser, the shape of the trench plan can be determined according to the displacement data gathered by the transducers, and is drawn in Figure 34. The trench plan was bell-mouth-shaped with a maximum width of 0.48 D, which also coincided with the in situ trench. After the water was pumped out, the developed trench could be observed, as shown in Figure 35.

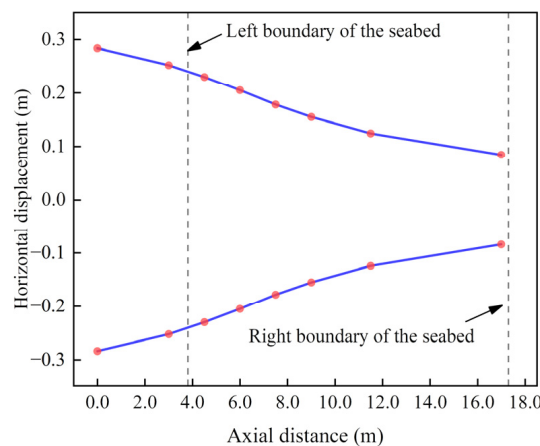


Figure 34. Lateral displacement range of the model SCR.



Figure 35. Developed trench shape.

5. Conclusions

In this study, a novel experimental platform was proposed and constructed to conduct dynamic loading tests of a truncated model SCR within the TDZ. The platform was constituted of a reinforced concrete soil tank, a loading system, and a soil stirring system. Detailed equipment and structures were introduced to make a better illustration of the feasibility of the test. The parameters adopted in this experiment were based on an in situ SCR. The layout of instrumentations and test loading conditions were designed to monitor the dynamic mechanical behavior of the model SCR and determine the influence of riser–soil interaction. Numerical simulations based on the vector form intrinsic finite element method were also conducted for comparison with the test results. According to the test and simulation results, the conclusions can be summarized as follows.

(1) The bending moment and vertical and horizontal cyclic displacement loads can be applied individually or simultaneously during the dynamic test of truncated model SCR within the TDZ. The elastic support can provide restraint to the tail end of the riser. Test clay soil can be prepared with the help of the soil stirring system and vacuum preloading system.

(2) The arrangement of the instrumentation is capable of reflecting the displacement and stress distribution along the model SCR. Based on the data gathered during the dynamic loading test, the mechanical behavior of the model SCR was analyzed, and the effect of loading amplitude and frequency were investigated. The stress range at the front of the model riser increased by more than 100% when the vertical displacement amplitude increased from 200 mm to 300 mm, whereas the loading frequency had only little influence, since the stress range only differed by less than 5%.

(3) The statical configuration, bending moment distribution, and time history of stress at different positions of SCR were compared between the numerical simulation and test results. High similarities proved the correctness and reliability of the nonlinear soil model and the VFIFE method.

(4) The maximum stress occurred when the riser was lowered. If the vertical loading amplitude was small, the minimum stress occurred when the riser was uplifted to the top. However, with the increase in vertical loading amplitude, the minimum stress within the middle of SCR happened when the riser penetrated deeper into the seabed, which may have also induced a larger stress range. The horizontal seabed resistance would vary the out-of-plane stress distribution of the SCR when the lateral displacement loads were applied.

(5) A trench with a ladle-shaped profile and a bell-mouth-shaped plan was developed during the test, and its shape was similar to the in situ trench. The maximum depth and width of the trench were 0.71 D and 0.48 D, respectively. Except for the cyclic displacement loads, the bending moment also contributed to the trench formation by increasing the deformation of SCR near the loading end.

Author Contributions: Conceptualization, Y.Y. and S.X.; methodology, S.X. and J.Y.; software, S.X.; validation, S.X., P.L. and X.L.; formal analysis, S.X. and L.X.; investigation, S.X. and P.L.; resources, Y.Y. and S.X.; data curation, S.X.; writing—original draft preparation, S.X.; writing—review and editing, S.X.; visualization, L.X.; supervision, Y.Y.; project administration, J.Y.; funding acquisition, J.Y. All authors have read and agreed to the published version of the manuscript.

Funding: This research was funded by The National Natural Science Foundation of China (Grant No. 51879189) and National Natural Science Foundation of China (Grant No. 52071234).

Institutional Review Board Statement: Not applicable.

Informed Consent Statement: Not applicable.

Data Availability Statement: The data presented in this study are available upon request from the corresponding author.

Conflicts of Interest: The authors declare no conflict of interest.

References

1. Yu, Y.; Xu, S.; Yu, J.; Xu, W.; Xu, L.; Xu, L. Dynamic Analysis of Steel Catenary Riser on the Nonlinear Seabed Using Vector Form Intrinsic Finite Element Method. *Ocean Eng.* **2021**, *241*, 109982. [[CrossRef](#)]
2. Drumond, G.P.; Pasqualino, I.P.; Pinheiro, B.C.; Estefen, S.F. Pipelines, Risers and Umbilicals Failures: A Literature Review. *Ocean Eng.* **2018**, *148*, 412–425. [[CrossRef](#)]
3. Quéau, L.M.; Kimiaei, M.; Randolph, M.F. Analytical Estimation of Static Stress Range in Oscillating Steel Catenary Risers at Touchdown Areas and Its Application with Dynamic Amplification Factors. *Ocean Eng.* **2014**, *88*, 63–80. [[CrossRef](#)]
4. Zargar, E.; Kimiaei, M.; Randolph, M. A New Hysteretic Seabed Model for Riser-Soil Interaction. *Mar. Struct.* **2019**, *64*, 360–378. [[CrossRef](#)]
5. Bai, X.; Huang, W.; Vaz, M.A.; Yang, C.; Duan, M. Riser-Soil Interaction Model Effects on the Dynamic Behavior of a Steel Catenary Riser. *Mar. Struct.* **2015**, *41*, 53–76. [[CrossRef](#)]
6. Randolph, M.; Quiggin, P. Non-Linear Hysteretic Seabed Model for Catenary Pipeline Contact. In *Volume 3: Pipeline and Riser Technology*; ASMEDC: New York, NY, USA, 1 January 2009; pp. 145–154.
7. Aubeny, C.; Biscontin, G. Interaction Model for Steel Compliant Riser on Soft Seabed. *SPE Proj. Facil. Constr.* **2008**, *3*, 1–6. [[CrossRef](#)]
8. Chen, J.; Bai, X.; Vaz, M.A. Dynamic Behavior of Steel Catenary Riser at the TDZ Considering Soil Stiffness Degeneration and Trench Development. *Ocean Eng.* **2022**, *250*, 110970. [[CrossRef](#)]
9. Elostá, H.; Huang, S.; Incecik, A. Trenching Effects on Structural Safety Assessment of Integrated Riser/Semisubmersible in Cohesive Soil. *Eng. Struct.* **2014**, *77*, 57–64. [[CrossRef](#)]
10. Bridge, C.D.; Howells, H.A. Observations and Modeling of Steel Catenary Riser Trenches. In Proceedings of the International Offshore and Polar Engineering Conference, Lisbon, Portugal, 1–6 July 2007; pp. 803–813.
11. Wang, K.; Low, Y.M. A Simple Parametric Formulation for the Seabed Trench Profile beneath a Steel Catenary Riser. *Mar. Struct.* **2016**, *45*, 22–42. [[CrossRef](#)]
12. Shiri, H. Influence of Seabed Trench Formation on Fatigue Performance of Steel Catenary Risers in Touchdown Zone. *Mar. Struct.* **2014**, *36*, 1–20. [[CrossRef](#)]
13. Mekha, B.; Randolph, M.; Bhat, S.; Jain, S. Modeling the Touchdown Zone Trench and Its Impact on SCR Fatigue Life. In Proceedings of the Offshore Technology Conference, Houston, TX, USA, 6 May 2013.
14. Yu, Y.; Xu, S.; Yu, J.; Xu, W.; Xu, L.; Xu, L. Influence of Seabed Trench on the Structural Behavior of Steel Catenary Riser Using the Vector Form Intrinsic Finite Element Method. *Ocean Eng.* **2022**, *251*, 110963. [[CrossRef](#)]
15. Shoghi, R.; Shiri, H. Modeling Touchdown Point Oscillation and Its Relationship with Fatigue Response of Steel Catenary Risers. *Appl. Ocean Res.* **2019**, *87*, 142–154. [[CrossRef](#)]
16. Shoghi, R.; Pesce, C.P.; Shiri, H. Influence of Trench Geometry on Fatigue Response of Steel Catenary Risers by Using a Boundary Layer Solution on a Sloped Seabed. *Ocean Eng.* **2021**, *221*, 108447. [[CrossRef](#)]
17. Willis, N.R.T.; West, P.T.J. Interaction between Deepwater Catenary Risers and a Soft Seabed: Large Scale Sea Trials. In Proceedings of the Offshore Technology Conference, Houston, TX, USA, 30 April 2001.
18. Bai, X.; Vaz, M.A.; Morooka, C.K.; Xie, Y. Dynamic Tests in a Steel Catenary Riser Reduced Scale Model. *Ships Offshore Struct.* **2017**, *12*, 1064–1076. [[CrossRef](#)]
19. Wang, L.; Zhang, J.; Yuan, F.; Li, K. Interaction between Catenary Riser and Soft Seabed: Large-Scale Indoor Tests. *Appl. Ocean Res.* **2014**, *45*, 10–21. [[CrossRef](#)]
20. Hodder, M.S.; Byrne, B.W. 3D Experiments Investigating the Interaction of a Model SCR with the Seabed. *Appl. Ocean Res.* **2010**, *32*, 146–157. [[CrossRef](#)]
21. Wang, L.Z.; Li, K.; Yuan, F. Lateral Cyclic Interaction between Catenary Riser and Soft Seabed. *Appl. Ocean Res.* **2017**, *63*, 11–23. [[CrossRef](#)]

22. Dai, Y.; Zhou, J. Experimental Investigations on Seismic Response of Riser in Touchdown Zone. *Int. J. Nav. Archit. Ocean Eng.* **2018**, *10*, 348–359. [[CrossRef](#)]
23. Tianfeng, Z.; Shixiao, F.; Tianhao, W. Seabed Stiffness Influences and Water Damping Effects on Vibration of the Touchdown Zone in a Steel Catenary Riser. *Int. J. Press. Vessel. Pip.* **2019**, *170*, 30–39. [[CrossRef](#)]
24. Bhattacharyya, A.; Tognarelli, M.; Li, G.; Ghosh, R.; Clukey, E.C.; Sun, Q. Simulation of SCR Behaviour at Touchdown Zone- Part I: Numerical Analysis of Global SCR Model Versus Sectional SCR Model. In Proceedings of the Offshore Technology Conference, Houston, TX, USA, 4 October 2011.
25. Elliott, B.J.; Zakeri, A.; Macneill, A.; Phillips, R.; Clukey, E.C.; Li, G. Centrifuge Modeling of Steel Catenary Risers at Touchdown Zone Part I: Development of Novel Centrifuge Experimental Apparatus. *Ocean Eng.* **2013**, *60*, 200–207. [[CrossRef](#)]
26. Elliott, B.J.; Zakeri, A.; Barrett, J.; Hawlader, B.; Li, G.; Clukey, E.C. Centrifuge Modeling of Steel Catenary Risers at Touchdown Zone Part II: Assessment of Centrifuge Test Results Using Kaolin Clay. *Ocean Eng.* **2013**, *60*, 208–218. [[CrossRef](#)]
27. Clukey, E.C.; Tognarelli, M.; Li, G.; Ghosh, R.; Phillips, R.D.; Zakeri, A.; Elliott, B.; Bhattacharyya, A.; Sun, Q. Simulation of SCR Behaviour at Touchdown Zone-Part II: Testing of a Sectional SCR Model in a Geotechnical Centrifuge. In Proceedings of the Offshore Technology Conference, Houston, TX, USA, 4 October 2011.
28. Hu, H.J.E.; Leung, C.F.; Chow, Y.K.; Palmer, A.C. Centrifuge Modelling of SCR Vertical Motion at Touchdown Zone. *Ocean Eng.* **2011**, *38*, 888–899. [[CrossRef](#)]

Disclaimer/Publisher’s Note: The statements, opinions and data contained in all publications are solely those of the individual author(s) and contributor(s) and not of MDPI and/or the editor(s). MDPI and/or the editor(s) disclaim responsibility for any injury to people or property resulting from any ideas, methods, instructions or products referred to in the content.